Downloaded from orbit.dtu.dk on: Nov 07, 2026

DTU Library

Immune protection and persistence in Pseudomonas aeruginosa infections by pyruvate cross-feeding

Lampadariou, Stefanos; Laborda, Pablo; Masiero, Lorenzo; Molin, Søren; Johansen, Helle Krogh; La Rosa, Ruggero

Published in:
Nature Communications

Link to article, DOI:
10.1038/s41467-026-75330-z

Publication date:
2026

Document Version
Publisher's PDF, also known as Version of record

Link back to DTU Orbit

Citation (APA):
Lampadariou, S., Laborda, P., Masiero, L., Molin, S., Johansen, H. K., & La Rosa, R. (2026). Immune protection and persistence in *Pseudomonas aeruginosa* infections by pyruvate cross-feeding. *Nature Communications*, *17*(1), Article 8428. https://doi.org/10.1038/s41467-026-75330-z

General rights
Copyright and moral rights for the publications made accessible in the public portal are retained by the authors and/or other copyright owners and it is a condition of accessing publications that users recognise and abide by the legal requirements associated with these rights.

- Users may download and print one copy of any publication from the public portal for the purpose of private study or research.
- You may not further distribute the material or use it for any profit-making activity or commercial gain
- You may freely distribute the URL identifying the publication in the public portal

If you believe that this document breaches copyright please contact us providing details, and we will remove access to the work immediately and investigate your claim.

nature communications

Article

https://doi.org/10.1038/s41467-026-75330-z

Immune protection and persistence in *Pseudomonas aeruginosa* infections by pyruvate cross-feeding

Received: 4 December 2025

Accepted: 22 June 2026

Published online: 08 July 2026

Check for updates

Stefanos Lampadariou[1,5], Pablo Laborda[2,5] ✉, Lorenzo Masiero[3], Søren Molin[1], Helle Krogh Johansen[2,3,4] & Ruggero La Rosa[2,3] ✉

Chronic infections by *Pseudomonas aeruginosa* in people with cystic fibrosis are characterized by persistent inflammation and oxidative stress, yet the mechanisms enabling bacterial persistence are not fully understood. Here, we identify a persistence mechanism mediated by pyruvate secretion resulting from mutations in the pyruvate dehydrogenase complex in clinical isolates of *P. aeruginosa*, with putative analogous mutations also identified in *Staphylococcus aureus*, *Haemophilus influenzae* and *Stenotrophomonas maltophilia*. These mutations lead to elevated extracellular pyruvate, which dampens host inflammatory responses and favors bacterial persistence. Pyruvate exerts multiple roles: scavenges reactive oxygen species such as H_2O_2, suppresses host immune activation both in airway epithelial cells and macrophages, and increases bacterial survival during phagocytosis. This metabolic crosstalk promotes bacterial persistence while reducing epithelial and macrophage inflammatory responses. Our findings reveal pyruvate as a bacterial immunometabolite that mimics host antioxidant defenses, reshaping the infection niche to favor long-term colonization. This work highlights the broader role of secreted metabolites in host-pathogen interactions and suggests new strategies targeting metabolic pathways to manage chronic infections.

Metabolism, the intricate network of biochemical reactions within a cell, is the foundation of life. Far from being a passive background process, metabolism actively supports every single cellular function, ensuring the constant supply of energy and building blocks necessary for growth[1]. In bacterial pathogens, metabolism plays an additional crucial role, directly influencing the ability to cause disease[2,3]. Indeed, metabolic pathways are increasingly recognized as key players in the establishment and progression of bacterial infections by controlling host damage and its immune response[4,5]. Strikingly, the precise and direct connections between specific metabolic pathways, the multifaceted mechanisms of bacterial pathogenicity, and the host response remain poorly understood[6].

Pseudomonas aeruginosa is an opportunistic pathogen causing both acute and chronic infections in immunocompromised patients[7]. Its ability to catabolize many carbon sources and colonize diverse environments and hosts reflects its extensive metabolic flexibility[8]. Interestingly, it has been shown that adaptive evolution within the airway of people with cystic fibrosis (pwCF) selects for specific metabolic features which provide increased fitness during the infection[9]. However, while the metabolic changes have been extensively described, the consequences of such metabolic specializations are largely unknown. One emerging hypothesis is that metabolic specialization promotes host–pathogen metabolic crosstalk leading to bacterial persistence[10,11] and altered host responses during infection[12]. The

[1]The Novo Nordisk Foundation Center for Biosustainability, Technical University of Denmark, Lyngby, Denmark. [2]Department of Clinical Microbiology 9301, Copenhagen Ø, Denmark. [3]Department of Health Technology, Technical University of Denmark, Lyngby, Denmark. [4]Department of Clinical Medicine, Faculty of Health and Medical Sciences, University of Copenhagen, Copenhagen, Denmark. [5]These authors contributed equally: Stefanos Lampadariou, Pablo Laborda. ✉e-mail: palama@dtu.dk; rugros@dtu.dk

ability of the host to limit the damage caused by pathogens without decreasing the bacterial load, defined as disease tolerance[12], has been associated with specific mechanisms of immune modulation during infection. For example, the immunometabolite itaconate mediates disease tolerance in *P. aeruginosa* pneumonia infection models by simultaneously inducing biofilm formation through alginate biosynthesis and limiting excessive inflammation by pulmonary glutamine assimilation[4,13]. This and other mechanisms of host–pathogen metabolic interactions could, therefore, constitute broader mechanisms of protection for bacterial pathogens[14]. This is even more relevant in persistent infections where the outcome is the maintenance of the infecting population for the long term rather than killing the host[15].

In pwCF, chronic *P. aeruginosa* infection is associated with sustained oxidative stress and excessive inflammation, primarily driven by reactive oxygen species (ROS) produced by neutrophils and macrophages. This process contributes to substantial tissue damage and progression of lung disease. Antioxidants are, therefore, necessary to maintain homeostasis and reduce inflammation. It has been proposed that the metabolite pyruvate, or its more stable form ethyl-pyruvate, elicits an antioxidant effect in several diseases due to its ability to react with H_2O_2, yielding acetate[16–18]. Moreover, it has been described that ethyl-pyruvate down-regulates the production of pro-inflammatory cytokines, such as interleukin-8 (IL-8)[19]. Interestingly, in several bacterial species, pyruvate has been described as a metabolic intermediate involved in pathogens' protection from H_2O_2 and virulence regulation[20–25]. However, whether pyruvate produced by bacterial pathogens modulates the immune system response and reduces the oxidative stress to promote persistence is unclear. We hypothesize that this mechanism could influence bacterial persistence through metabolic crosstalk and host immunomodulation. This would help the establishment of a persistent slow-growing bacterial population, such as that present in pwCF, by modulating oxidative stress and host immune responses.

Here, we provide evidence that pyruvate dehydrogenase complex (PDHc) mutations lead to high secretion of pyruvate, which in the host microenvironment elicits a triple role. First, pyruvate directly reacts non-enzymatically with ROS species, such as H_2O_2, protecting the bacterial community from oxidative killing. Secondly, it influences the host response by limiting IL-8 secretion by the airway epithelial cells, suppressing immune system cells recruitment. Third, it limits macrophage activation and increases bacterial survival within the phagolysosome. Indirectly, these mechanisms reduce oxidative stress and inflammatory activation in the infection microenvironment, thereby promoting bacterial persistence. This is supported by the broad distribution of PDHc mutations in several clinical isolates of *P. aeruginosa*, *Staphylococcus aureus*, *Haemophilus influenzae,* and *Stenotrophomonas maltophilia*. Altogether, these results suggest that PDHc mutations are selected for in persisting bacterial infections and influence bacterial persistence within the host through a generalized mechanism of metabolic crosstalk.

Results

Pyruvate dehydrogenase mutations protect against H_2O_2 stress

We hypothesized that mutations in the *P. aeruginosa aceEF* operon, encoding the PDHc, arising during chronic infections in pwCF[26], lead to pyruvate secretion as a protection mechanism against ROS due to the ability of pyruvate to react with H_2O_2[27–29]. To assess this hypothesis, we employed, along with the laboratory reference strain PAO1, two mutant strains, one harboring a point mutation in the *aceE* gene, leading to a Phe > Ser amino acid change at position 184, and the other one a 4 bp insertion in the *aceF* gene leading to a frameshift starting from Lys 273[26]. As previously reported, the *aceE* and *aceF* strains secrete pyruvate during growth in the defined medium SCFM2, which recreates the metabolic composition of sputum samples from pwCF and which does not contain pyruvate. Additionally, these strains show a fitness cost of the mutations underlined by their reduced growth rate[26].

To assess the neutralizing reactivity of pyruvate against H_2O_2, we performed a H_2O_2 killing assay using an air-liquid interface (ALI) model system consisting of mucociliated, differentiated airway epithelial cells that mimic the human airway environment. This system allows for the investigation of host responses, including epithelial integrity and cytokine production during infection. ALI models were infected on the apical side with PAO1 or the *aceF* mutant strain for 6 h to allow for the establishment of a bacterial population, followed by the addition of H_2O_2 on the apical side, and incubated for an extra 30 min in the presence or absence of pyruvate. Bacterial colony forming units (CFUs) from the planktonic fraction (apical compartment) and those attached to the epithelium were quantified to verify the bactericidal activity of H_2O_2 and the protective effect of pyruvate (Fig. 1A). As hypothesized, the addition of H_2O_2 significantly reduced the CFUs in both fractions, while the addition of pyruvate provided complete protection of the bacterial population (two-way ANOVA with Tukey's multiple comparisons test, $p < 0.05$). It is worth noting that in the apical side of the ALI models infected with the *aceF* mutant strain, no pyruvate was detected after 6 h of infection before the addition of H_2O_2, indicating that pyruvate was either not secreted under the tested ALI conditions at a level within the detection limit, or that pyruvate was immediately assimilated by epithelial cells (Fig. S1A). Therefore, we added exogenous pyruvate even for the *aceF* strain. The neutralizing effect of pyruvate against H_2O_2 is, thus, independent of the bacterial strain used, its growth capacity, and the associated infection pattern.

To further evaluate this neutralizing function in immune cells, we performed cytokine profiling by multiplex flow cytometry after induction with H_2O_2 in the presence or absence of pyruvate in human peripheral blood monocyte-derived macrophages, which are central for long-term airway immunity in CF airways. While H_2O_2 exposure led to an increased secretion of IL-6, IL-8, and IL-10 cytokines as a consequence of the extracellular oxidative stress, levels returned to baseline with pyruvate, confirming the absence of stress under neutralizing conditions (Fig. 1B; one-way ANOVA with Tukey's multiple comparisons test, $p < 0.05$).

To further characterize pyruvate activity against H_2O_2 on the bacterial physiology, we measured the growth rate and lag phase of PAO1, *aceE,* and *aceF* strains in SCFM2 in the presence or absence of H_2O_2 and pyruvate (Figs. 1C and S1B, C). H_2O_2 significantly impaired growth and extended the lag phase in all strains, while pyruvate restored both parameters (Figs. 1C and S1B, C; two-way ANOVA with Tukey's multiple comparisons test, $p < 0.05$). Similarly, in an H_2O_2 killing assay, *aceE* and *aceF* mutants showed higher survival than PAO1, while PAO1 supplemented with *aceF* supernatant showed comparable protection (Fig. 1D; one-way ANOVA with Tukey's multiple comparisons test, $p > 0.05$). This result agrees with the pyruvate secretion profile of the strains, where the *aceE* mutant showed transient secretion, while the *aceF* continuous secretion (Fig. 1E). Since pyruvate reacts with H_2O_2 to form acetate, which can complement PDHc mutations[26,30], we observed that acetate produced by the neutralizing reaction between pyruvate and H_2O_2 increased the growth rate of the *aceF* mutant but not that of PAO1 or the *aceE* strain (Fig. S1D). A similar effect was seen in LB medium, which contains traces of acetate[31,32] (Fig. S1E).

These results indicate that pyruvate can protect against H_2O_2 oxidative stress both in in vivo-like infection environments and in laboratory conditions.

Reduced virulence and immune cell recruitment during airway infection

Metabolic crosstalk in host–pathogen interactions is a particularly fundamental process since the availability and competition for nutrients can influence the physiology of both the infecting bacteria and the

https://doi.org/10.1038/s41467-026-75330-z

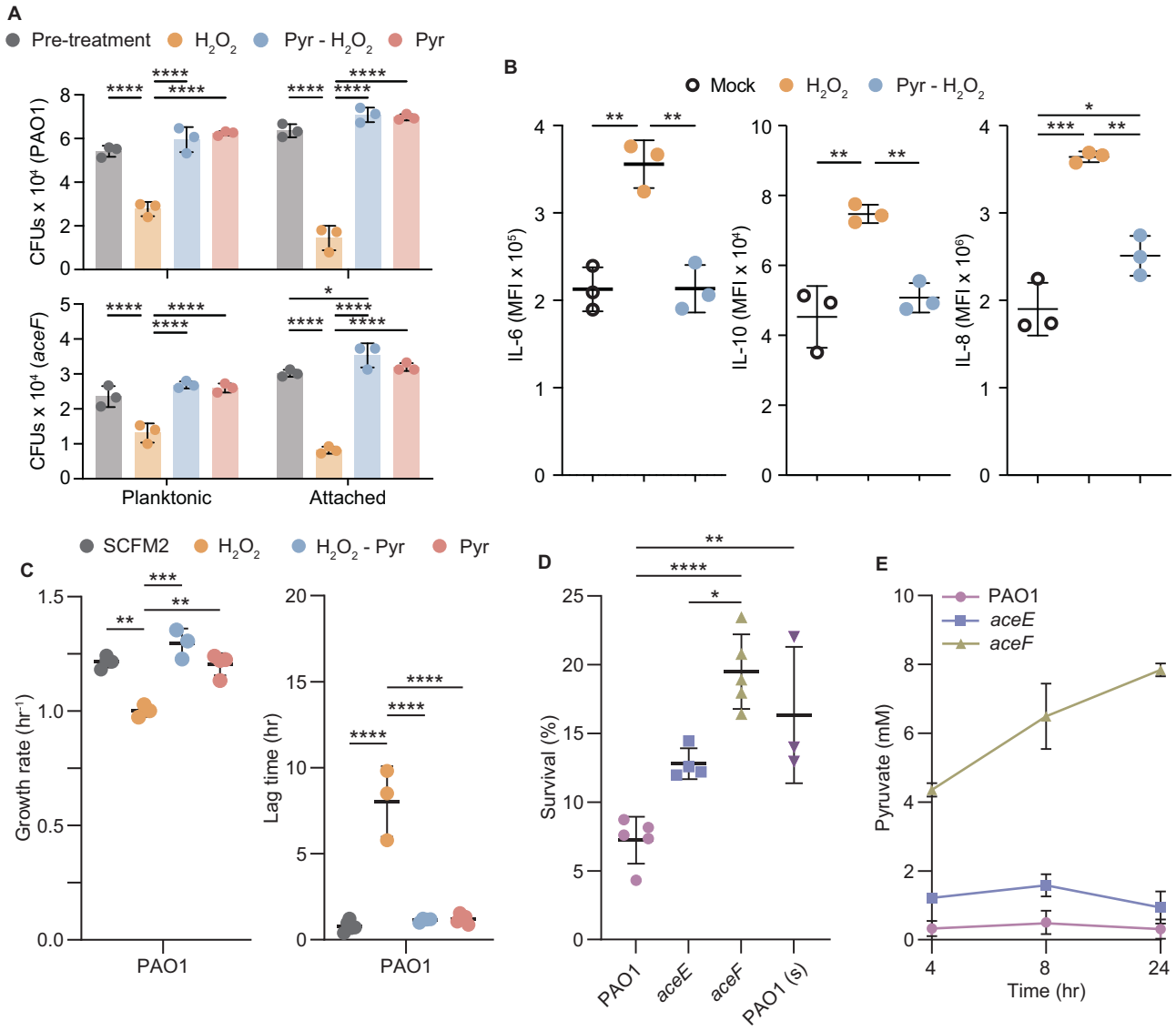

Fig. 1 | Neutralizing effect of pyruvate on H_2O_2 in in vivo-like models and laboratory conditions. A Colony forming units (CFUs) of PAO1 and the *aceF* mutant strain before and after H_2O_2 exposure in air-liquid interface (ALI) infection models of fully differentiated BCi-NS1.1 cells, with apical supplementation of 10 µL drops of 2 mM H_2O_2 and 10 mM pyruvate. CFUs were quantified both for the planktonic bacteria in the apical compartment and attached to the epithelium. **B** Cytokine release upon oxidative stress induction with 5 mM H_2O_2 in the presence or absence of 5 mM of pyruvate in primary macrophages. Data are presented as mean fluorescence intensity (MFI). **C** Growth rate (h^{-1}) and lag time of PAO1 strain cultured in SCFM2 medium supplemented with 5 mM H_2O_2, in the presence or absence of 5 mM pyruvate. **D** Survival percentage following 5 mM H_2O_2 exposure in SCFM2 medium for PAO1, *aceE*, and *aceF* mutant strains, and PAO1 supplemented with the *aceF* strain's supernatant (PAO1 (s)). **E** Pyruvate concentration (mM) in the supernatant of PAO1, *aceE*, and *aceF* mutant cultures after 4, 8, and 24 h of incubation in SCFM2. In all panels, data are presented as mean ± SD from at least three biological replicates. Each icon represents a biological replicate. Except for (**A**), where two-way ANOVA was used, statistical significance was determined using one-way ANOVA with Tukey's multiple comparisons test. Significance is indicated as * ($p < 0.05$), ** ($p < 0.01$), *** ($p < 0.001$), and **** ($p < 0.0001$). Source data are provided as a Source data file.

host. To assess whether pyruvate secretion by the *aceE* and *aceF* mutant strains changes the virulence potential of the infecting bacteria and the host response, we conducted infection assays using ALI infection models (Fig. 2).

Since the *aceF* mutant strain has a reduced growth rate relative to PAO1 in laboratory conditions (Fig. S1B), we performed infection assays and quantified infection parameters after 16 h of infection and additionally at 24 h for the *aceF* mutant strain. The additional 24 h time point for the *aceF* mutant was included to ensure that bacterial loads were comparable between strains and allow a more accurate comparison of infection parameters by minimizing confounding effects due to differences in growth kinetics. To quantify bacterial cytotoxicity and colonization capacity, we measured transepithelial electrical resistance (TEER), which reflects epithelial barrier integrity, and bacterial CFUs in the ALI infection models. CFUs were assessed for bacteria growing as planktonic cells in the apical compartment, those firmly attached to the epithelium, and those present in the basolateral compartment after penetration through the epithelium.

TEER measurements revealed a lower capacity of the *aceF* mutant strain to damage the epithelium after 24 h compared to PAO1 after 16 h of infection. In contrast, the *aceE* mutant strain induced a comparable epithelial damage to that of PAO1 (Fig. 2A), suggesting that this mutation does not impair bacterial cytotoxicity. However, the bacterial CFUs were significantly lower for both mutant strains relative to PAO1, indicating a clear fitness cost of these PDHc mutations in in vivo-like conditions (Fig. 2B). Additionally, the *aceF* mutant strain triggered significantly lower IL-8 secretion compared to PAO1 and the *aceE* mutant strain (Fig. 2C), a key cytokine involved in immune cell

https://doi.org/10.1038/s41467-026-75330-z

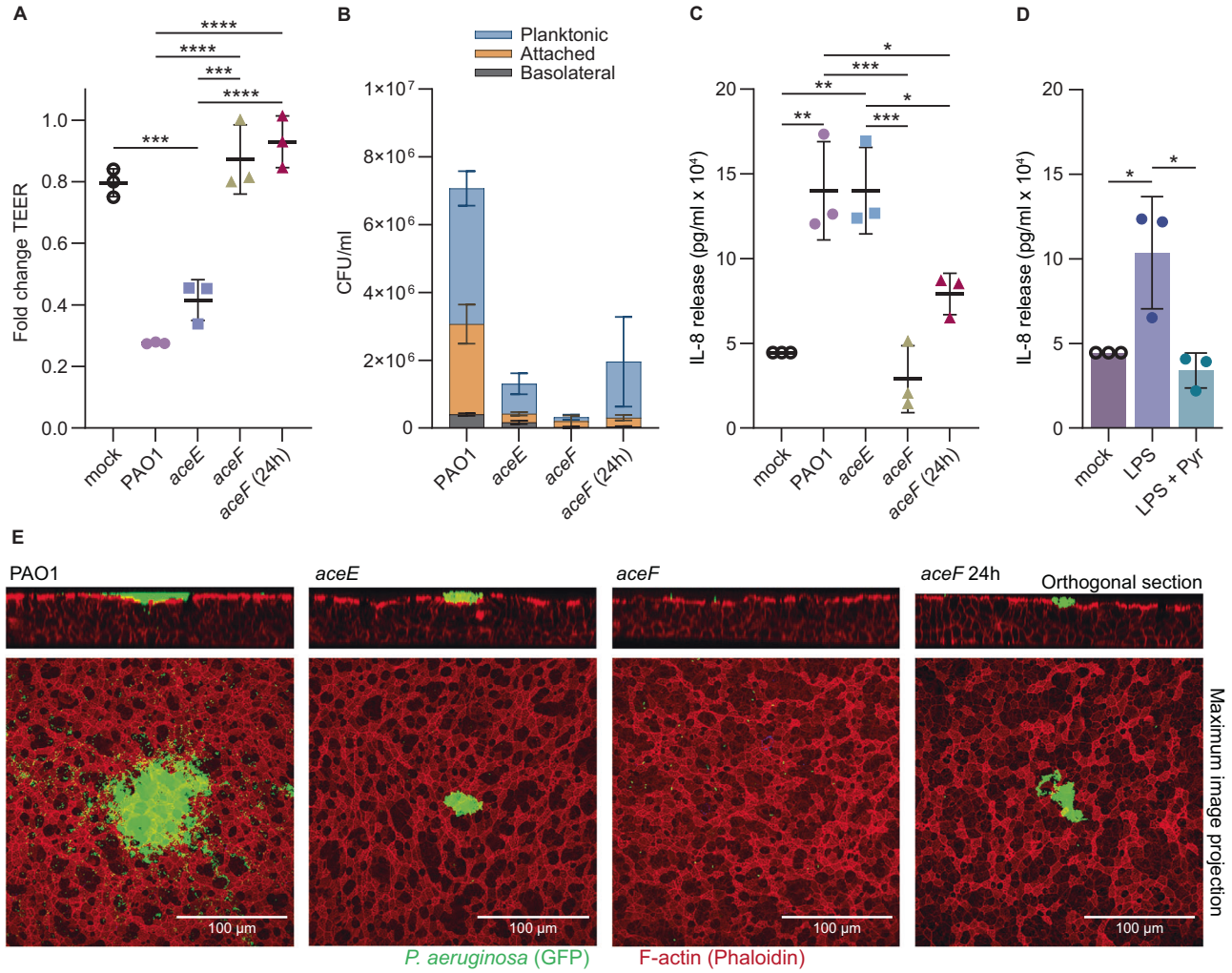

Fig. 2 | Mutations in *aceE* and *aceF* influence the airway infection dynamics of *P. aeruginosa*. **A** Fold change in transepithelial electrical resistance (TEER), **B** bacterial counts (CFUs) for bacteria growing as planktonic cells in the apical compartment, those firmly attached to the epithelium, and those present in the basolateral compartment, and **C** Interleukin-8 (IL-8) secretion following 16 h of infection with PAO1, *aceE*, and *aceF* mutant strains, and after 24 h for the *aceF* strain, using an air-liquid interface (ALI) model of fully differentiated BCi-NS1.1 airway cells. **D** IL-8 secretion into the basolateral medium following stimulation with 10 µL of 100 µg/mL LPS and inhibition with 10 µL of 10 mM pyruvate (100 nmol). "Mock" refers to uninfected control cells. Statistical significance was determined using one-way ANOVA with Tukey's multiple comparisons test for TEER and IL-8 quantification. Significance is indicated as *($p < 0.05$), **($p < 0.01$), ***($p < 0.001$), and ****($p < 0.0001$). Data represent the mean ± SD from three biological replicates, each with three technical replicates, and icons represent each biological replicate. Source data are provided as a Source data file. **E** Confocal microscopy images of fully differentiated ALI models infected with *P. aeruginosa* PAO1, *aceE,* or *aceF* for 16 h and *aceF* for 24 h, expressing GFP in green, and the epithelial actin stained with phalloidin in red. The results shown were consistently obtained in at least three independent biological replicates of the experiment. Scale bar = 100 µm.

recruitment at the site of infection (two-way ANOVA with Tukey's multiple comparisons test, $p < 0.05$). Notably, extensive transepithelial penetration (CFUs in the basolateral side) was only observed for PAO1, whereas *aceE* and *aceF* mutant strains did not exhibit such an invasive phenotype, potentially indicating a reduction in their virulence (Fig. 2B). These results were further supported by confocal microscopy analysis, which revealed distinct colonization patterns between PAO1, *aceE*, and *aceF* on the airway epithelial surfaces (Fig. 2E).

As the 24 h infections with the *aceF* mutant strain exhibited similar bacterial growth to the 16 h infection with the *aceE* mutant strain, but a significantly lower epithelial damage and IL-8 secretion, we hypothesized that the secreted pyruvate might also elicit immunosuppression activity on the epithelial cells. To investigate this hypothesis, we stimulated the epithelium by adding lipopolysaccharide (LPS), which elicits a strong immune response, and tested the effect of pyruvate on IL-8 secretion (Fig. 2D). Interestingly, we observed a significant reduction of IL-8 release in the presence of LPS + pyruvate as compared to LPS alone, along with complete pyruvate assimilation over the course of the assay (Figs. 2D and S1F, one-way ANOVA with Tukey's multiple comparisons test, $p < 0.05$). These findings support our hypothesis that pyruvate can additionally act as an immunosuppressor on the airway epithelium.

These results suggest that mutations in the *aceE* and *aceF* genes may contribute to persistent infections and establish a potential link between pyruvate metabolism, virulence regulation, and modulation of the immune system recruitment in *P. aeruginosa* infections.

Pyruvate modulates macrophage killing capacity and limits cytokine release

Macrophages constitute one of the first lines of defense against airway infection and are central for long-term airway immunity in CF airways. Since ALI infections revealed reduced IL-8 secretion upon infection with the *aceF* strain, we hypothesize that pyruvate secretion may modulate macrophage responses.

https://doi.org/10.1038/s41467-026-75330-z

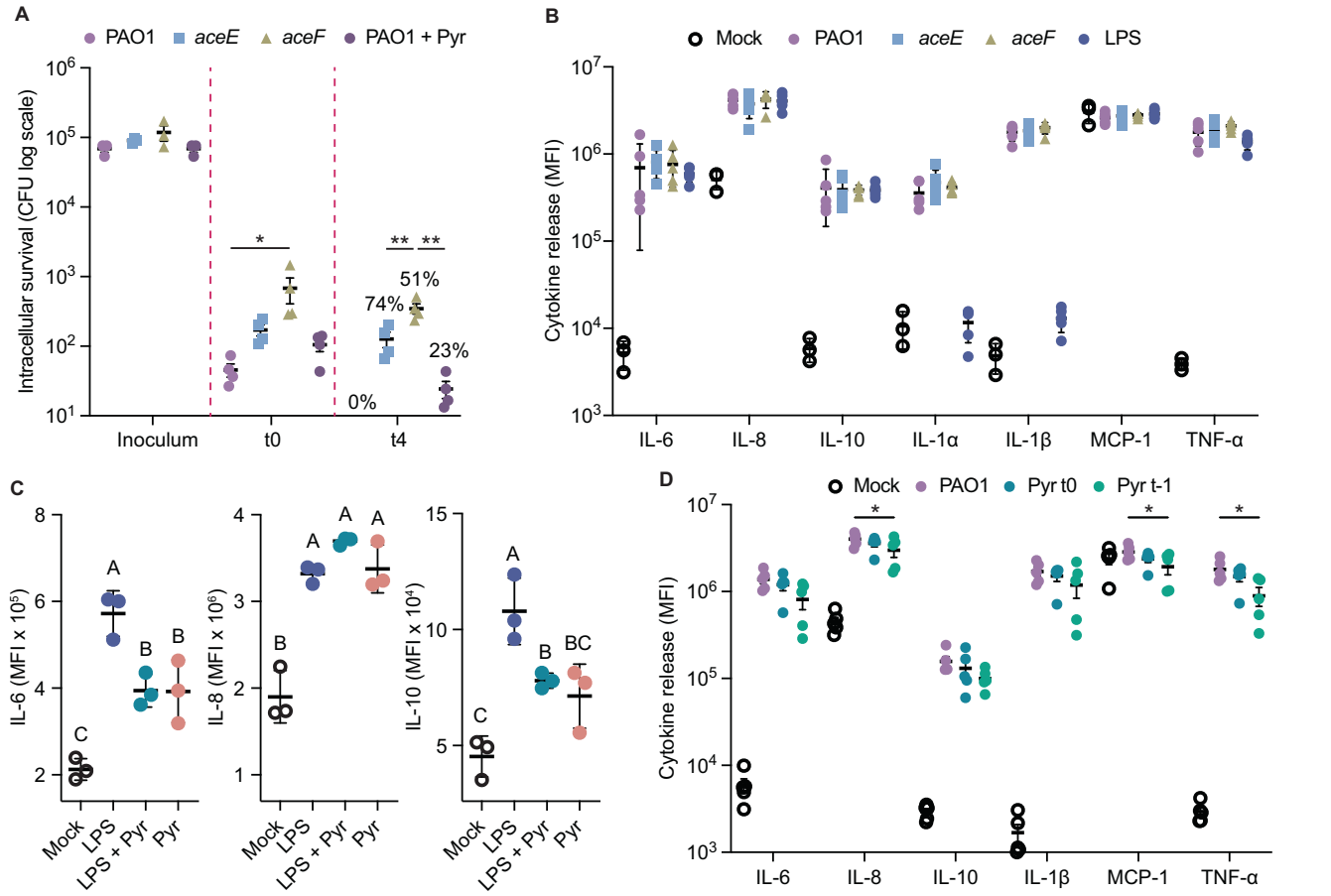

Fig. 3 | Pyruvate reduces macrophage activation and limits bacterial killing. **A** Intracellular bacterial survival upon macrophage phagocytosis of PAO1, *aceE,* and *aceF* strains. For PAO1 + Pyr, 5 mM of pyruvate was added at the time of infection. Inoculum represents the bacterial count before infection, t0 represents the time point after 1 h bacterial phagocytosis followed by 1 h gentamycin treatment to remove extracellular bacteria, and t4 represents the time point where intracellular bacterial survival was quantified. Survival is reported as the percentage of CFUs quantified at t0 relative to those quantified at t4. **B** Cytokine release upon infection with PAO1, *aceE,* and *aceF* strains. LPS was used as a positive control of macrophage stimulation. **C** IL-6, IL-8, and IL-10 release upon stimulation with LPS in the presence and absence of 5 mM of pyruvate. **D** Cytokine release upon infection with PAO1 in the presence or absence of 5 mM of pyruvate. Pyruvate was added either at the time of infection (t0), or macrophages were pre-incubated for 1 h prior infection (t-1). For cytokine stimulation assays, data are presented as mean fluorescence intensity (MFI). Statistical significance was determined using one-way (**A**, **C**) or two-way (**B**, **D**) ANOVA with Tukey's multiple comparisons test. Significance is indicated as *($p < 0.05$), **($p < 0.01$), or by connecting letters, where groups labeled with different letters differ significantly ($p < 0.05$) (**C**). Data represent the mean ± SEM from at least three biological replicates, and icons represent each biological replicate. Source data are provided as a Source data file.

To test this hypothesis, we performed infection assays using human primary monocyte-derived macrophages and quantified both phagocytic bacterial killing and macrophage activation by cytokines release (Fig. 3). Killing assays revealed that *aceE* and *aceF* mutant strains were more resistant to intracellular killing with a large fraction of phagocytosed bacteria (51–74% survival) remaining viable within the macrophages after 4 h of infection (Fig. 3A; one-way ANOVA with Tukey's multiple comparisons test, $p < 0.05$). In contrast, no PAO1 CFUs were detected at the same timepoint (0% survival), consistent with the already lower intracellular CFUs quantified at t0, when bacteria had undergone a 1 h incubation followed by a 1 h gentamicin treatment to eliminate extracellular cells. As intramacrophage killing begins within the first 15–30 min of phagocytosis, the increased survival of the *aceF* strain relative to PAO1 was already apparent at t0 (Fig. 3A). Importantly, supplementation with pyruvate at the time of PAO1 infection led to an increased bacterial survival (23% survival), supporting pyruvate's role in promoting survival to macrophage killing (Fig. 3A; one-way ANOVA with Tukey's multiple comparisons test, $p < 0.05$). Additionally, complementation of the *aceE* strain by chromosomal integration (Tn7 site) of a single wild-type copy of *aceE* under its native promoter (*aceE(rev)* strain)[26] resulted in a significant reduction in survival, from 74 to 54%, confirming the role of PDHc in bacterial survival within macrophages (Fig. S1G; unpaired t-test, $p = 0.0241$).

Despite these differences in bacterial survival, macrophages infected with PAO1, *aceE*, or *aceF* for 4 h showed comparable cytokine profiles for IL-6, IL-8, IL-10, IL-1α, IL-1β, MCP-1, and TNF-α (Fig. 3B; one-way ANOVA with Tukey's multiple comparisons test, $p > 0.05$). However, when assessing pyruvate secretion by the *aceE* and *aceF* strains under the infection conditions, we found that no pyruvate could be quantified within the short time frame of the experiment (Fig. S1H). As for the ALI infections, this result suggests that either pyruvate was not secreted by the *aceE* and *aceF* mutants under the infection conditions at a level within the detection limit, or that it was rapidly internalized by macrophages. Nevertheless, pyruvate was assimilated by macrophages when stimulated with LPS in the presence of 5 mM of exogenous pyruvate (Fig. S1I, one-way ANOVA with Tukey's multiple comparisons test, $p < 0.001$), supporting the hypothesis that pyruvate might be readily assimilated if secreted by the *aceE* and *aceF* strains. While low concentrations of pyruvate, potentially secreted by the mutant bacteria, may be insufficient to modulate cytokine release directly, even a small amount of pyruvate could readily react with H_2O_2 within the phagolysosome, thereby enhancing bacterial survival.

To further evaluate the role of pyruvate in immune cell activation, we stimulated macrophages with LPS in the presence or absence of exogenous pyruvate. While LPS triggered a classic inflammatory response characterized by increased IL-6 and IL-10, pyruvate addition suppressed secretion of both cytokines (one-way ANOVA with Tukey's multiple comparisons test, $p < 0.05$), while no difference was instead observed for IL-8 (Fig. 3C; one-way ANOVA with Tukey's multiple comparisons test, $p > 0.05$). A similar result was obtained when infecting macrophages with PAO1 in presence of exogenous pyruvate either added at the time of infection (Pyr t0), or by pre-incubating macrophages for one hour with pyruvate (Pyr t-1), where pre-incubation decreased the release of IL-8, MCP-1 and TNF-α relative to untreated PAO1 infections (Fig. 3D; one-way ANOVA with Tukey's multiple comparisons test, $p < 0.05$). Other cytokines showed a similar decreasing trend, albeit the differences did not reach statistical significance.

Together, these results indicate that pyruvate secretion enhances bacterial survival within macrophages and dampens macrophage activation by reducing the release of key pro-inflammatory cytokines.

Clinical relevance of PDHc mutations

The PDHc, composed of the E1 (AceE) decarboxylase, the E2 (AceF) dihydrolipoyl transacetylase, and the E3 (Lpd) dehydrogenase components, is central to directing pyruvate into the TCA cycle[33]. To assess the consequences of PDHc mutations and their role in metabolic crosstalk during infection, we selected from our longitudinal collection of *P. aeruginosa* clinical isolates from pwCF having persistent infections, 12 clinical strains each containing a different non-synonymous mutation in the PDHc encoding genes *aceE* and *aceF*[34]. The selected strains represent diverse clone types from different pwCF and are representative of the 89 isolates in our collection containing PDHc mutations (Fig. 4A)[34]. Mutations in the *aceE* gene (E1 component) were mostly located in the decarboxylation/transketolase_N domain, while mutations in the *aceF* gene (E2 component) were mostly located within the multiple lipoyl domain.

To determine whether these strains exhibit a similar phenotype to the recombinant *aceE* and *aceF* mutant strains, we measured their maximum growth rate and pyruvate secretion during growth in SCFM2 medium. The growth rate showed a significant variability, with a range from 0.321 to 1.234, indicating a broad fitness cost of the mutations (Fig. 4B). Additionally, all clinical strains secreted high amounts of pyruvate during growth (Fig. 4C), with concentrations comparable to those of the recombinant strains (2–8 mM; Fig. 1E) and previously analyzed clinical strains[26,35]. As observed for the *aceE* and *aceF* mutant strains, two distinct patterns of pyruvate secretion were observed: one involving the transient secretion followed by either re-assimilation or extracellular catabolism to a different metabolite, and another one characterized by continuous secretion for at least 24 h (Fig. 4C). The relationship between the secretion patterns and the type or location of mutations remains unclear, as both point mutations and insertion-deletion events occur in the *aceE* and *aceF* genes, independently of the secretion pattern.

To confirm the functional role of PDHc mutations in clinical isolates, we selected two paired sets of clinical isolates, each consisting of one wild-type isolate and its corresponding PDHc mutant derivative. These pairs belonged to the clone types DK08 (*aceE* SNP C671G) and DK19 (*aceF* nonsense G7T), isolated from two different pwCF within 3 months (DK08) and 5 months (DK19), respectively, and differing by only a few additional mutations[34] (Fig. 4A and Supplementary Data S1). Notably, in macrophage survival assays, the PDHc mutant strains showed markedly higher intracellular survival (46–84%) compared to their paired wild type counterparts (11–14%) (one-way ANOVA with Tukey's multiple comparisons test, $p < 0.0001$), confirming that these mutations confer a substantial survival advantage also in clinical isolates (Fig. 4D). It is worth noting that the observed differences in survival between PDHc mutant strains (353 vs. 346) could depend on the functional impact of each mutation, or on the historical contingency of the individual evolutionary trajectories of the strains. Nevertheless, these results confirm the extent of the metabolic crosstalk between *P. aeruginosa* and the host in different infection scenarios and bacterial lineages.

Since pyruvate is a central metabolite conserved across diverse species[23,36], we hypothesized that similar mutations in the PDHc might also arise in other pathogens associated with persistent infections. To test this possibility, we aligned all complete sequences of the PDHc subunits E1 and E2 from *S. aureus*, *H. influenzae*, *S. maltophilia,* and *P. aeruginosa* available on the National Center for Biotechnology Information (NCBI) database. We observed greater variability in subunit E2, particularly in the form of high-impact mutations (insertions, deletions, or frameshifts), which were frequently detected in strains with metadata confirming a clinical origin, both in *P. aeruginosa* (Supplementary Fig. 2) and in the other species (Fig. 4E). In contrast, high-impact mutations in subunit 1 were less common, and only some *S. aureus* strains with such mutations could be traced back to clinical isolates (Supplementary Fig. 2). Mutations ranged from 1 to 23 amino acid deletions to 1–12 amino acid insertions. In *H. influenzae*, mutations predominantly affected the multiple lipoyl domain of the E2 dihydrolipoyl transacetylase; in *S. aureus*, they clustered within the E1 decarboxylation/transketolase N domain; and in *S. maltophilia*, they occurred mainly in the linker region connecting the lipoyl domain to the E2 catalytic core[33] (Fig. 4A, E). Since these indel mutations arise at a similar location to the mutations accumulated by *P. aeruginosa* (Fig. 4A), their disruptive nature makes them likely to impair the PDHc catalytic activity, thereby potentially leading to pyruvate accumulation. However, in-depth experimental characterization of their metabolic consequences would be required to link altered PDHc activity to persistence during infection with *S. aureus*, *H. influenzae*, or *S. maltophilia*. It is important to note that additional functionally relevant PDHc mutations may exist in clinical strains, since our targeted analysis was restricted only to clearly defined high-impact variants associated with clinical metadata. Overall, these findings indicate that PDHc mutations are not restricted to *P. aeruginosa* but are also present in clinical isolates of other prevalent airway pathogens.

Discussion

Metabolism is a fundamental process dynamically regulated to meet the nutrient availability and physiological demands of an organism. In *P. aeruginosa*, clinical isolates have been shown to undergo metabolic specialization during infection, suggesting adaptive responses to the host environment[9,35,37]. These shifts not only compensate for the fitness costs of other phenotypic traits but can also be actively selected to enhance bacterial persistence[26].

During infections caused by wild-type *P. aeruginosa*, bacteria employ the T3SS, which damages the host epithelium and, in turn, induces IL-8 secretion to recruit immune cells[38]. Once recruited, activated macrophages produce a respiratory burst and phagocytose the invading bacteria (Fig. 5A). In this study, we investigated mutations in the *aceE* and *aceF* genes, encoding components of the PDHc, as a non-conventional persistence mechanism during chronic *P. aeruginosa* airway infection, altering such infection pattern[26,34]. These mutations prevent efficient processing of pyruvate, revealing that secreted pyruvate functions not just as a metabolic byproduct but as a bacterial immunometabolite that reshapes the host environment to favor persistence. We demonstrate that pyruvate exerts several functions at the host–pathogen interface (Fig. 5B). First, it scavenges ROS through a non-enzymatic reaction, potentially reducing oxidative stress in the airway microenvironment[39]. Second, it limits IL-8 production, likely reducing the host immune response and the recruitment of immune cells. Third, it limits macrophage activation and enhances bacterial survival after phagocytosis. Chronic activation of innate immune cells

https://doi.org/10.1038/s41467-026-75330-z

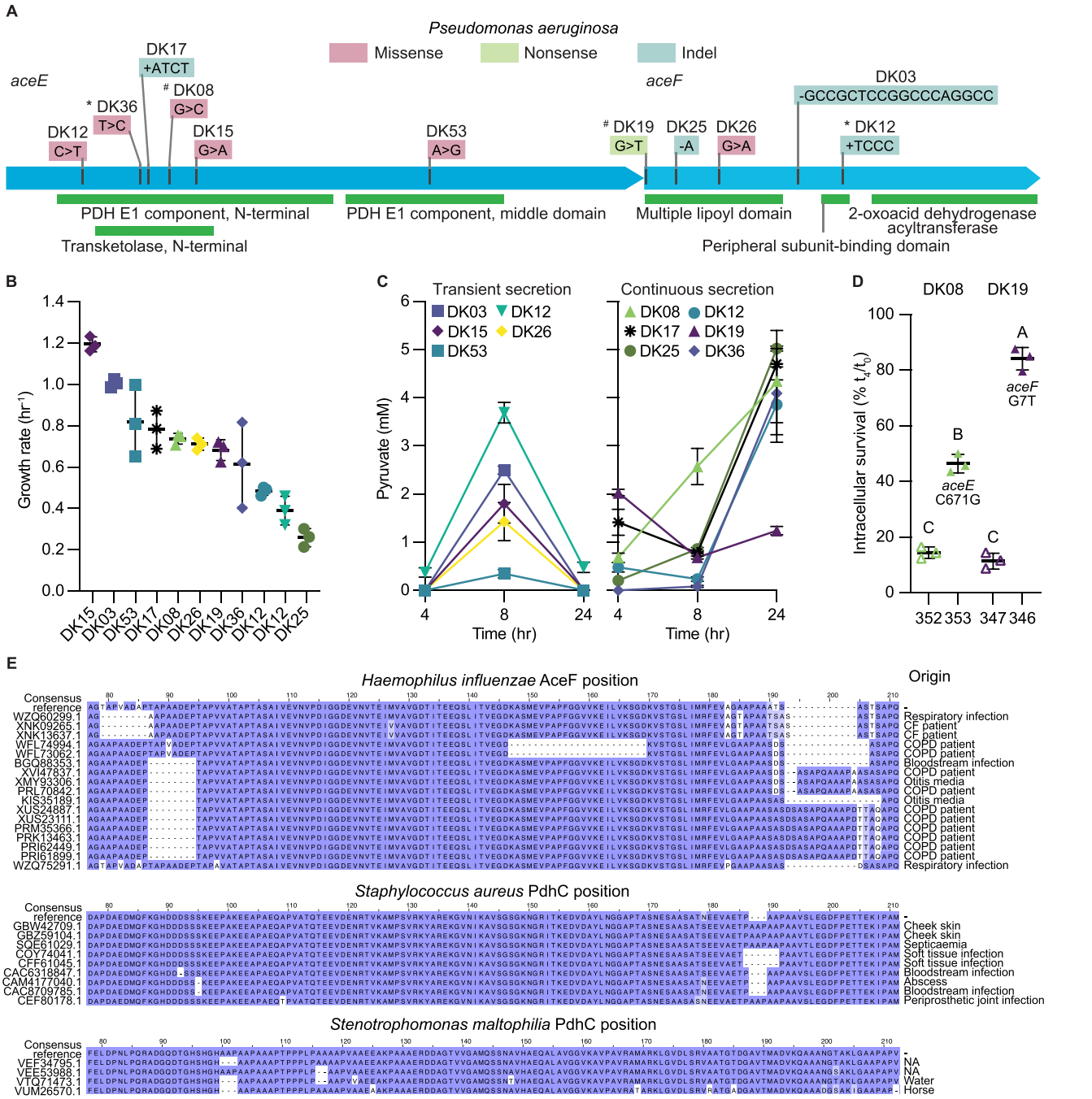

Fig. 4 | Characterization of clinical strains with mutations in the PDHc. A Types of non-synonymous mutations observed in the *aceEF* operon in different clinical isolates from chronically infected pwCF belonging to different clone types. The functional domains of the E1 (*aceE*) and E2 (*aceF*) components of the PDHc are indicated. The * indicates the mutation present in the PAO1-derived recombinant strains *aceE* and *aceF*, while the # indicates the mutations present in the clinical isolates 353 and 346 (**D**). **B** Growth rate (hour^{-1}) in SCFM2 of clinical strains from distinct clone types, indicated as DK##, harboring PDHc mutations. Two independent mutations were identified in distinct isolates belonging to clone type DK12. Data represent the mean ± SD from three biological replicates, and icons represent each biological replicate. **C** Pyruvate secretion (mM) of clinical strains harboring PDHc mutations over 24 h of growth in SCFM2. The distinct patterns are indicated by transient and continuous secretion. Data represent the mean ± SEM of three independent biological replicates. **D** Intracellular bacterial survival upon macrophage phagocytosis of clinical strains 352 and 353 belonging to the clone type DK08 (green) and 347 and 346 belonging to the clone type DK19 (violet). Survival is reported as the percentage of CFUs quantified at t0 relative to those quantified at t4, where t0 represents the time point after 1 h bacterial phagocytosis followed by 1 h gentamycin treatment to remove extracellular bacteria, and t4 represents the time point where intracellular bacterial survival was quantified. Strain 353 and 346 (filled symbols) harbor, respectively, a SNP mutation (C671G) in the *aceE* gene and a nonsense SNP (G7T) in the *aceF* gene. Strains 352 and 347 contain a wild-type copy of the *aceEF* genes. Statistical significance was determined using one-way ANOVA with Tukey's multiple comparisons test, where groups labeled with different letters differ significantly ($p < 0.0001$). Data represent the mean ± SD from three biological replicates, and icons represent each biological replicate. **E** Multiple sequence alignments of PDHc subunit 2 proteins from *Haemophilus influenzae*, *Staphylococcus aureus*, and *Stenotrophomonas maltophilia*. Sequences were selected based on the presence of high-impact mutations and traceable clinical metadata, except for *S. maltophilia*, for which all sequences harboring high-impact mutations were included regardless of metadata availability. The color code is based on the BLOSUM62 matrix. Source data are provided as a Source data file.

https://doi.org/10.1038/s41467-026-75330-z

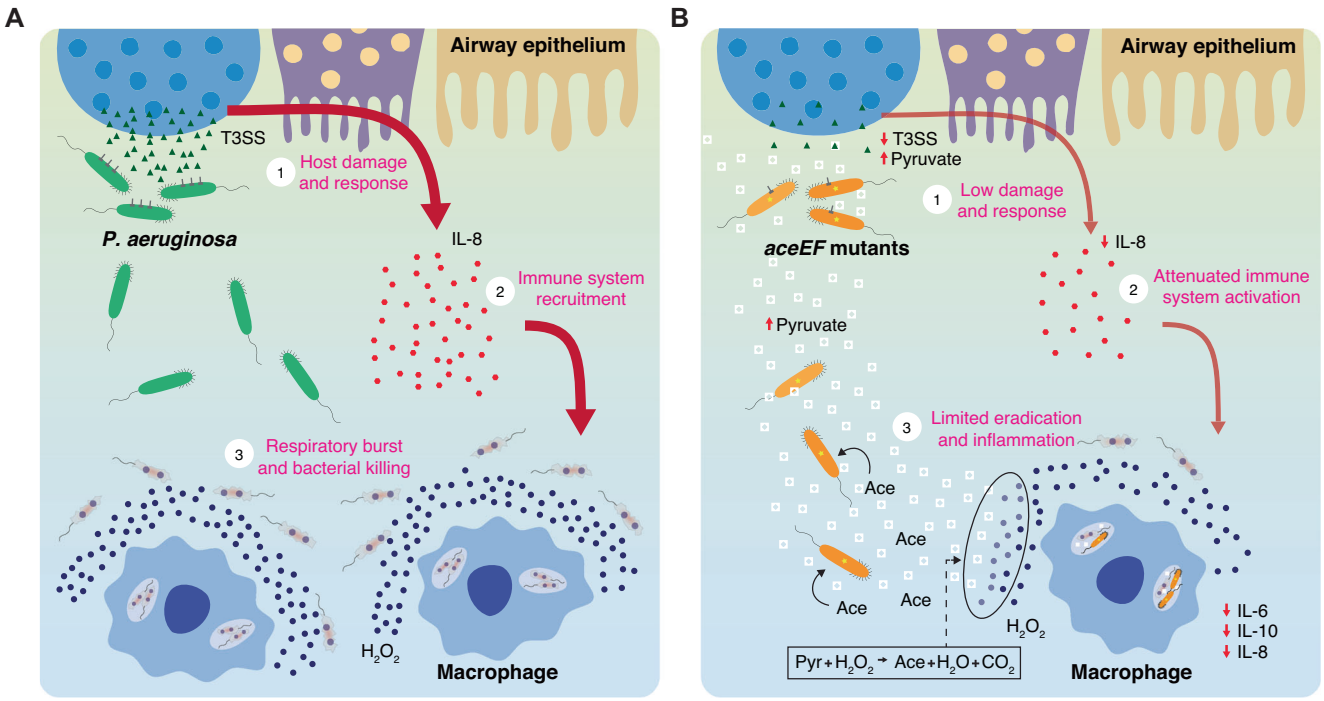

Fig. 5 | Persistence mechanism through PDHc mutations in *P. aeruginosa*. **A** Infection dynamics of wild-type strains: (1) the secretion of T3SS causes damage to the airway epithelium and consequently elicits a host response; (2) the host secretes IL-8 for immune system recruitment; (3) macrophages reach the infection site and produce ROS, including H_2O_2, to eradicate the extracellular and intracellular (phagolysosome) infecting bacteria. **B** Infection dynamics of the *aceE* and *aceF* mutant strains: (1) reduced T3SS activity and the secretion of pyruvate lead to a reduced damage and host response; (2) low levels of secreted IL-8 by epithelial cells and of secreted IL-6, IL-8 and IL-10 by macrophages cause an attenuated immune response; (3) fewer innate immune cells arrive at the infection site to produce ROS which is neutralized by the pyruvate present in the environment; intracellular bacteria increase their survival within the phagolysosomes by pyruvate release; acetate is produced as by-product of the pyruvate-H_2O_2 reaction which can be assimilated by PDHc mutant strains compensating for their low growth rate.

and epithelial dysfunction in infected CF airways generates sustained ROS levels[40]. While the antioxidant roles of pyruvate have been well described in mammalian systems[16–18], in this case, pyruvate secretion by the pathogen attenuates oxidative killing and inflammation, effectively hijacking a metabolic circuit used by the host to protect its own tissues. Notably, the reaction of pyruvate with H_2O_2 yields acetate, which may be re-assimilated by PDHc mutant strains and shuttled into the TCA cycle, partially compensating for their metabolic deficit[30]. However, this could potentially increase the bacterial biomass, triggering inflammation. This suggests a potential dual role of pyruvate in supporting both immune modulation and bacterial metabolic adaptation, although the net impact on bacterial burden and inflammation likely depends on the infection context.

Oxidative stress within the host environment may, therefore, represent a key selective pressure driving the emergence of *aceEF* mutations. However, when *P. aeruginosa* has experimentally evolved under oxidative stress in laboratory conditions, the predominant adaptive response involves mutations that lead to overexpression of catalases[41]. While pyruvate reacts non-enzymatically with H_2O_2, catalases achieve a similar antioxidant outcome through an enzymatic reaction[42]. This difference in selection dynamics suggests that, although both mechanisms reduce oxidative burden, *aceEF* mutations may not merely reflect a response to oxidative pressure, but rather a broader adaptation to the host environment. Consistent with this result, our findings show that secreted pyruvate not only neutralizes ROS but also reduces IL-8 secretion by airway epithelial cells, dampens macrophage activation, and promotes bacterial survival after phagocytosis. Importantly, this effect is independent of the downregulation of classical virulence pathways. As previously described, PDHc mutants exhibit hallmarks of chronic infection, including reduced expression of the T3SS, upregulation of T6SS, or increased production of phenazines[7,26,43]. While T3SS suppression likely contributes to reduced host immune activation since its effectors can induce inflammatory responses[44], our data show that pyruvate alone can reduce cytokine production. Still, further analyses are required to identify the specific selective pressures driving the accumulation of PDHc mutations during infection and to fully disentangle the molecular links between immune suppression, persistence, virulence, and macrophage metabolic remodeling following pyruvate exposure. Nevertheless, the conserved increase in intracellular macrophage survival observed in both recombinant laboratory strains and clinical isolates with distinct evolutionary histories and infection scenarios underscores the clinical relevance of this mechanism and its link to persistence.

Immune activation requires a profound metabolic reprogramming that both supports and defines effector functions[45]. Pyruvate lies at the core of this process, as its metabolic fate determines the balance between glycolytic and oxidative metabolism. In this context, exogenous pyruvate, here produced by infecting bacteria, can perturb this delicate equilibrium, disrupting the metabolic reprogramming required for immune activation and thereby dampening the host immune response through a still unclear mechanism[46,47]. This immunomodulatory effect of pyruvate may contribute to bacterial persistence by reducing inflammatory responses despite the continued presence of the pathogen. Our findings conceptually parallel the previously described itaconate–alginate interplay in *P. aeruginosa*, which has been reported to limit immunopathology[4,13]. However, our study extends this paradigm by identifying pyruvate as a universally conserved and central metabolite with immune modulator function. Unlike alginate, which is species-specific, pyruvate can be secreted by a wide range of bacteria under metabolic stress or imbalance. This observation raises the possibility that pyruvate immune modulation

may contribute to chronic colonization in other pathogens as well[22,23]. Moreover, in situ analyses of sputum samples from pwCF showed a decrease in expression of the PDHc, indicating that a similar effect could potentially also be achieved through regulatory mechanisms[48]. Given its dual role in metabolism and signaling, pyruvate may have broader and underappreciated effects on immune regulation beyond airway infections[19].

While the clinical relevance of this mechanism is supported by the widespread accumulation and long-term maintenance of PDHc mutations in clinical isolates from pwCF, it is important to note that a more in-depth molecular characterization of pyruvate metabolism in whole organisms and in vivo models would substantially advance our understanding of how these mutations contribute to persistence and disease progression, insights that cannot be fully captured with the in vitro systems used in this study. Additionally, functional characterization of the macrophage reduced inflammation, whether through TCA cycle/OXPHOS stimulation, itaconate induction, or M2 polarization via α-ketoglutarate enrichment[5], could reveal new immunomodulatory markers with relevance not only for CF but also for other chronic infections and inflammatory diseases. While we identified high-impact mutations in the PDHc in publicly available sequences of clinical strains of *S. aureus*, *H. influenzae,* and *S. maltophilia* from infection sites not restricted to chronic infections, the actual functional consequences of these mutations remain unverified. Nonetheless, they provide preliminary evidence of potential convergent evolutionary trajectories during infection in other bacterial species. For example, the functional role of the PDHc and pyruvate metabolism during infection could constitute a recurrent feature of pathogen adaptation during infection, as shown in *S. aureus* infections, where secretion of the lipoyl-E2 component of the PDHc prevents macrophage activation by reducing Toll-like receptor 1/2 activation by bacterial lipopeptides[49,50].

More broadly, our work emphasizes the emerging role of secreted metabolites as signaling molecules in host–pathogen interactions. Future studies should explore whether pyruvate is part of a broader repertoire of metabolites with immunomodulatory effects. It will also be important to assess whether interfering with pyruvate-mediated signaling, by limiting its secretion, counteracting its effects or restoring host redox balance, could offer novel strategies for managing chronic infections without relying solely on antimicrobial therapies. Ultimately, targeting such metabolic pathways may impair bacterial persistence, providing a complementary approach to conventional antimicrobial strategies.

Methods

Strains and media

The *aceE* and *aceF* mutant strains in a *P. aeruginosa* PAO1 background used in this study were previously generated in ref. 26, and clinical strains used in this work were previously described in ref. 34. The local ethics committee at the Capital Region of Denmark (Region Hovedstaden) approved the use of the stored *P. aeruginosa* isolates (registration number H-21078844). Bacteria were grown in SCFM2 medium prepared as previously described in ref. 51, excluding DNA and mucins to reduce viscosity, or in LB medium. Cultures were grown at 37 °C and 250 rpm.

Bacterial growth assays

Bacterial growth was assessed at 37 °C and 250 rpm in a BioTek ELx808 Absorbance Microtiter Reader (BioTek Instruments, Winooski, Vermont, USA) by measuring $OD_{600\,nm}$ every 20 min for 24 h. Growth was initiated by inoculating an overnight bacterial culture in LB or SCFM2 media supplemented with either 5 mM H_2O_2, 5 mM pyruvate, 5 mM acetate, or the pre-incubated reaction at 37 °C and 250 rpm for 30 min of 5 mM H_2O_2 with 5 mM pyruvate.

Pyruvate concentration determination

Bacterial cultures were initiated at $OD_{600\,nm} = 0.01$ in SCFM2. The supernatants were collected by centrifugation at 5000 × *g* for 10 min at 4, 8, and 24 h after inoculation. For the quantification of pyruvate in the respective supernatants, the Pyruvate Assay Kit (Sigma-Aldrich) was used following the manufacturer's instructions.

H_2O_2 killing assays

H_2O_2 killing assays were performed as previously described[52], with minor modifications. Late exponential phase cultures ($OD_{600\,nm} \approx 2.5$) in SCFM2 were normalized with the supernatant of an overnight culture of the same strain to an $OD_{600\,nm}$ of 0.5. 5 mM H_2O_2, or 5 mM H_2O_2 together with 5 mM of pyruvate, were incubated with the normalized cultures. After 30 min, 0.2% (w/v) sodium thiosulfate was added to neutralize residual H_2O_2. CFUs were determined by the standard microdilution technique on LB agar plates. Survival was reported as a percentage of CFUs counted in the treated sample relative to the CFUs counted in the samples before treatment.

Air-liquid interface infection model preparation

BCi-NS1.1 cells, a human airway basal cell line with immortalized properties and the ability to differentiate into secretory, goblet, Clara, and ciliated cells under ALI conditions[53], were utilized to establish ALI infection models, as previously described[54,55]. Initially, the cells were expanded in culture flasks maintained at 37 °C with 5% CO_2 in a humidified incubator, using Pneumacult-Ex Plus medium (STEMCELL Technologies) as per the manufacturer's guidelines. Following expansion, 10^5 cells were seeded onto polyester membrane inserts (1 µm pore size, Falcon) pre-coated with type I collagen (Gibco). Once confluency was achieved, ALI conditions were induced by removing the medium from the apical chamber and replacing the basolateral medium with Pneumacult-ALI maintenance medium (STEMCELL Technologies), supplemented with 4 µg/mL heparin, 480 ng/mL hydrocortisone, Pneumacult-ALI supplement, and Pneumacult-ALI maintenance supplement (STEMCELL Technologies). The ALI cultures were maintained at 37 °C and 5% CO_2 in a humidified incubator for 28 days, with media replenished every 3–4 days. TEER was routinely monitored using a chopstick electrode (STX2; World Precision Instruments) to assess epithelial polarization. After 15 days of ALI culture, accumulated mucus was cleared by washing the apical surface with PBS every 7 days.

Epithelial infection procedure and characterization

A 10 µL drop of diluted overnight culture, containing 10^3 CFUs, was applied to the apical surface of fully differentiated BCi-NS1.1 ALI cultures, with 600 µL of supplemented Pneumacult-ALI maintenance medium present in the basolateral chamber. Control wells received an equivalent volume of bacteria-free PBS. The infected cells were incubated at 37 °C with 5% CO_2 in a humidified incubator for the required duration to assess the infection. After incubation, 200 µL of PBS was added to the apical surface, and TEER measurements were recorded as described above. Fold-change TEER values (after *vs* before infection) below 1 indicated reduced barrier integrity and epithelial damage. The 200 µL of PBS from the apical side and the 600 µL of medium from the basolateral chamber were collected, and bacterial CFUs in these samples were quantified by plating 10 µL of serial dilutions onto LB agar plates. The remaining samples were stored at −80 °C for future analysis. At this stage, the cells were either prepared for bacterial CFU counting on the epithelium or for imaging via confocal microscopy. For CFU quantification, 200 µL of PBS was added to the apical surface, and the epithelial layer was disrupted using a cell scraper. The resulting suspension was then subjected to LB agar plating of 10 µL in serial dilutions to determine CFU counts.

To prepare infected ALI cultures for confocal microscopy, samples were rinsed once with PBS and fixed with 4% paraformaldehyde,

which was added to both the apical and basolateral chambers, for 20 min at 4 °C. Following fixation, cells were washed three times with PBS, then permeabilized and blocked by incubating them in a buffer containing 3% BSA, 1% saponin, and 1% Triton X-100 in PBS for 1 h at room temperature. A 100 µL staining solution containing Phalloidin-AF555 (Invitrogen) diluted at 1:400 in a staining buffer (3% BSA and 1% saponin in PBS) was applied to the apical chamber. The cells were then incubated for 2 h at room temperature for staining. Fixed and stained epithelial layers were carefully detached from their supports using a scalpel and mounted onto glass slides with VECTASHIELD Antifade Mounting Medium (VWR). Imaging of infected cultures was performed using a Leica Stellaris 8 Confocal Microscope (×40 magnification, 1.3 oil) and analyzed with LasX software 1.4.4.26810 (Leica).

The basolateral media collected at the end of the infection was also used to measure IL-8 release, following the manufacturer's protocol for the Human IL-8/CXCL8 DuoSet ELISA Kit (R&D Systems).

H_2O_2 killing assays in ALI cultures

To assess the effectiveness of pyruvate in protecting bacteria colonizing the epithelial infection system from H_2O_2, the infection in fully differentiated ALI models was first established as previously described. After 6 h of incubation at 37 °C and 5% CO_2 in a humidified incubator, 10 µl of 2 mM H_2O_2 or first 10 µl of 5 mM pyruvate was added to the apical chamber, followed by 10 µl of 2 mM H_2O_2. The system was then further incubated at 37 °C and 5% CO_2 for an additional 30 min. Subsequently, 0.2% (w/v) sodium thiosulfate was added to neutralize residual H_2O_2, TEER was measured, and CFUs present in the apical chamber, basolateral medium, or attached to the epithelium were quantified by plating 10 µL of serial dilutions of respective bacterial suspensions on LB agar plates, as previously described. Finally, the percentage of bacterial survival was calculated by comparing CFU counts with those of untreated epithelial cultures.

Determination of epithelial IL-8 release inhibition by pyruvate

To induce the release of IL-8 by the epithelium, 1000 ng of LPS with or without 10 µl of 10 mM pyruvate were inoculated into the apical surface of fully differentiated ALI models. The basolateral media was collected after 16 h and IL-8 release was measured in those samples following the manufacturer's protocol for the Human IL-8/CXCL8 Duoset ELISA Kit (R&D Systems).

Macrophages preparation

Peripheral blood mononuclear cells (PBMCs) were isolated from fresh buffy coats obtained from healthy donors through the Department of Clinical Immunology, Blood Bank, at Rigshospitalet (Copenhagen, Denmark). This study was approved by the local ethics committee of the Capital Region of Denmark (Region Hovedstaden), registration number H-20024750. Buffy coats from 3 to 4 donors were pooled for each experiment to increase cell yield and reduce donor-specific variability. PBMCs were processed on the day of collection. Fifty milliliters of buffy coat were diluted 1:1 in PBS supplemented with 2% fetal bovine serum (FBS; Gibco). PBMCs were isolated using 50 mL LEUCOSEP tubes (Greiner) pre-filled with Lymphoprep (STEMCELL Technologies). After isolation, cells were washed twice in PBS + 2% FBS + 2 mM EDTA and centrifuged at 120 × *g* for 10 min at 4 °C to remove residual platelets. PBMCs were then cryopreserved at 1×10^7 cells/mL in FBS containing 10% dimethyl sulfoxide (DMSO; Thermo Fisher Scientific).

Cryopreserved PBMCs were rapidly thawed at 37 °C and immediately transferred into pre-warmed M0 base medium consisting of RPMI 1640 (Gibco) supplemented with 10% FBS and 50 ng/mL macrophage colony-stimulating factor (M-CSF; Miltenyi Biotec). Monocytes were purified by negative selection using the MojoSort™ Human Pan Monocyte Isolation Kit (BioLegend), according to the manufacturer's instructions. Purified monocytes were seeded at 1.4×10^7 cells/mL in M0 medium in P-100 tissue culture-treated dishes and maintained at 37 °C and 5% CO_2. Cells were differentiated into macrophages over 6 days, with a medium change at 24 h to remove non-adherent cells that were seeded in a new dish.

For macrophage harvesting, cultures were incubated with TrypLE (Gibco) for 5–10 min at 37 °C; cells were detached using a cell scraper, and TrypLE was neutralized with cold PBS. Macrophages were pelleted at 300 × *g* for 5 min and resuspended at the desired concentration. A total of 1.25×10^5 cells were seeded per well in 48-well clear flat-bottom tissue culture-treated plates (Falcon) and incubated for 24 h before downstream assays.

Macrophages induction assay

Before each experiment, the supernatant from macrophages seeded in 48-well plates was removed and replaced with 300 µL of fresh M0 medium. Macrophages were then stimulated with *P. aeruginosa* at a multiplicity of infection (MOI) of 1, H_2O_2 (5 mM), LPS (1 µg/mL), or the same conditions supplemented with pyruvate (5 mM), as indicated. After 4 h at 37 °C and 5% CO_2, supernatants were collected and stored at −80 °C. Cytokine levels were quantified using the Cytometric Bead Array Flex Set (CBA; BD Biosciences) for human IL-6, IL-8, IL-10, IL-1β, IL-1α, MCP-1, and TNF-α, in a NovoCyte Quanteon Flow Cytometer (Agilent) following the manufacturer's instructions. Three to five biological replicates were analyzed, each in technical triplicate, and a non-treated group served as the mock control.

Phagocytosis and intracellular survival assay

Before infection, the supernatant in each well was removed and replaced with 300 µL of fresh M0 medium. Macrophages were infected at a MOI of 1 with selected *P. aeruginosa* strains prepared from overnight cultures. The inoculum dose was verified by serial plating on LB agar. Immediately after infection, plates were centrifuged at 1200 × *g* for 5 min to promote bacterial contact with macrophages. To eliminate extracellular bacteria, gentamicin was added at 1 h post-infection (hpi) to a final concentration of 50 µg/mL.

For quantification of phagocytosis, cells were washed with PBS at 2 hpi and lysed in PBS containing 0.5% (v/v) Triton X-100. CFUs were determined by serial dilution and plating, representing the number of internalized bacteria.

Intracellular survival was assessed using a parallel plate infected with the same inoculum and macrophage batch. At 6 hpi, cells were washed with PBS and lysed in PBS + 0.5% (v/v) Triton X-100. CFUs obtained from serial dilutions reflected bacterial survival within macrophages after 6 h.

Protein alignments

Protein sequences corresponding to PDHc subunits 1 and 2 from *P. aeruginosa*, *S. aureus*, *H. influenzae*, and *S. maltophilia* were retrieved from the NCBI protein database, by the query "((*Pseudomonas aeruginosa*[Organism]) and aceE) not "partial"[Title]," "((*Pseudomonas aeruginosa*[Organism]) and aceF) not "partial"[Title]," "((*Staphylococcus aureus*[Organism]) and pdhA) not "partial"[Title]," "((*Staphylococcus aureus*[Organism]) and pdhC) not "partial"[Title]," "((*Haemophilus influenzae*[Organism]) and aceE) not "partial"[Title]," "((*Haemophilus influenzae*[Organism]) and aceF) not "partial"[Title]," "((*Stenotrophomonas maltophilia*[Organism]) and pdhA) not "partial"[Title]," "((*Stenotrophomonas maltophilia*[Organism]) and pdhC) not "partial"[Title]," respectively. Entries annotated as partial were excluded from the analysis. Multiple sequence alignments were performed using MAFFT software (v7)[56] with default parameters.

Quantification and statistical analyses

Growth rates and maxOD were calculated in the QurvE 1.1 software[57] by linear fitting during the exponential phase. Data were analyzed using GraphPad Prism 10.3.1 software (GraphPad Software). Statistically

significant differences were examined using ordinary one-way ANOVA or two-way ANOVA test with Tukey's multiple comparisons test to derive the significance of differences between all groups of each experiment. A p-value of <0.05 was considered statistically significant.

Reporting summary

Further information on research design is available in the Nature Portfolio Reporting Summary linked to this article.

Data availability

The authors declare that all data necessary for supporting the findings of this study are enclosed in this paper and provided in the Source data and Supplementary Data S1. Source data are provided with this paper.

References

1. Chubukov, V., Gerosa, L., Kochanowski, K. & Sauer, U. Coordination of microbial metabolism. *Nat. Rev. Microbiol.* **12**, 327–340 (2014).
2. Passalacqua, K. D., Charbonneau, M.-E. & O'Riordan, M. X. D. Bacterial metabolism shapes the host–pathogen interface. *Microbiol. Spectr.* **4**, 3 (2016).
3. Rohmer, L., Hocquet, D. & Miller, S. I. Are pathogenic bacteria just looking for food? Metabolism and microbial pathogenesis. *Trends Microbiol.* **19**, 341–348 (2011).
4. Chen, Y. T. et al. A host-pathogen metabolic synchrony that facilitates disease tolerance. *Nat. Commun.* **16**, 1–17 (2025).
5. Riquelme, S. A., Beg, A. Z., Lung, T. W. F. & Prince, A. Host–microbe interactions in the lung and the role of immunometabolism. in *Metabolites as Signals in Immunity and Inflammation* 7–26, https://doi.org/10.1016/B978-0-443-15447-8.00002-7. (Academic Press, 2025).
6. Bhagwat, A., Haldar, T., Kanojiya, P. & Saroj, S. D. Bacterial metabolism in the host and its association with virulence. *Virulence* **16**, 2459336 (2025).
7. Rossi, E. et al. *Pseudomonas aeruginosa* adaptation and evolution in patients with cystic fibrosis. *Nat. Rev. Microbiol.* **19**, 331–342 (2021).
8. Nikel, P. I., Martínez-García, E. & De Lorenzo, V. Biotechnological domestication of pseudomonads using synthetic biology. *Nat. Rev. Microbiol.* **12**, 368–379 (2014).
9. La Rosa, R., Johansen, H. K. & Molin, S. Adapting to the airways: metabolic requirements of *Pseudomonas aeruginosa* during the infection of cystic fibrosis patients. *Metabolites* **9**, 234 (2019).
10. La Rosa, R., Molin, S. & Johansen, H. K. *Pseudomonas aeruginosa*: persistence beyond antibiotic resistance. *Trends Microbiol.* **33**, 1076–1084 (2025).
11. La Rosa, R., Johansen, H. K. & Molin, S. Persistent bacterial infections, antibiotic treatment failure, and microbial adaptive evolution. *Antibiotics* **11**, 419 (2022).
12. McCarville, J. L. & Ayres, J. S. Disease tolerance: concept and mechanisms. *Curr. Opin. Immunol.* **50**, 88–93 (2018).
13. Riquelme, S. A. et al. *Pseudomonas aeruginosa* utilizes host-derived itaconate to redirect its metabolism to promote biofilm formation. *Cell Metab.* **31**, 1091–1106 (2020).
14. Wong Fok Lung, T. et al. *Klebsiella pneumoniae* induces host metabolic stress that promotes tolerance to pulmonary infection. *Cell Metab.* **34**, 761–774.e9 (2022).
15. Young, D., Hussell, T. & Dougan, G. Chronic bacterial infections: living with unwanted guests. *Nat. Immunol.* **3**, 1026–1032 (2002).
16. Yang, R., Zhu, S. & Tonnessen, T. I. Ethyl pyruvate is a novel anti-inflammatory agent to treat multiple inflammatory organ injuries. *J. Inflamm.* **13**, 37 (2016).
17. Kao, K. K. & Fink, M. P. The biochemical basis for the anti-inflammatory and cytoprotective actions of ethyl pyruvate and related compounds. *Biochem. Pharmacol.* **80**, 151–159 (2010).
18. Chakhtoura, M. et al. Ethyl pyruvate modulates murine dendritic cell activation and survival through their immunometabolism. *Front. Immunol.* **10**, 30 (2019).
19. Hollenbach, M. et al. Ethyl pyruvate and ethyl lactate down-regulate the production of pro-inflammatory cytokines and modulate expression of immune receptors. *Biochem. Pharmacol.* **76**, 631–644 (2008).
20. Bücker, R., Heroven, A. K., Becker, J., Dersch, P. & Wittmann, C. The pyruvate-tricarboxylic acid cycle node: a focal point of virulence control in the enteric pathogen *Yersinia pseudotuberculosis*. J. Biol. Chem. **289**, 30114–30132 (2014).
21. Redanz, S. et al. Pyruvate secretion by oral streptococci modulates hydrogen peroxide dependent antagonism. *ISME J.* **14**, 1074–1088 (2020).
22. Paulini, S. et al. The biological significance of pyruvate sensing and uptake in *Salmonella enterica* serovar Typhimurium. *Microorganisms* **10**, 1751 (2022).
23. Harper, L. et al. *Staphylococcus aureus* responds to the central metabolite pyruvate to regulate virulence. *mBio* **9**, e02272-17 (2018).
24. Abernathy, J., Corkill, C., Hinojosa, C., Li, X. & Zhou, H. Deletions in the pyruvate pathway of *Salmonella* Typhimurium alter SPI1-mediated gene expression and infectivity. *J. Anim. Sci. Biotechnol.* **4**, 5 (2013).
25. Troxel, B. et al. Pyruvate protects pathogenic spirochetes from H_2O_2 killing. *PLoS ONE* **9**, e84625 (2014).
26. Pedersen, B. H. et al. Metabolic specialization drives reduced pathogenicity in *Pseudomonas aeruginosa* isolates from cystic fibrosis patients. *PLoS Biol.* **22**, e3002781 (2024).
27. Andrae, U., Singh, J. & Ziegler-Skylakakis, K. Pyruvate and related alpha-ketoacids protect mammalian cells in culture against hydrogen peroxide-induced cytotoxicity. *Toxicol. Lett.* **28**, 93–98 (1985).
28. Wang, X. et al. Pyruvate protects mitochondria from oxidative stress in human neuroblastoma SK-N-SH cells. *Brain Res.* **1132**, 1–9 (2007).
29. Guarino, V. A., Oldham, W. M., Loscalzo, J. & Zhang, Y. Y. Reaction rate of pyruvate and hydrogen peroxide: assessing antioxidant capacity of pyruvate under biological conditions. *Sci. Rep.* **9**, 19568 (2019).
30. Jeyaseelan, K. & Guest, J. R. Isolation and properties of pyruvate dehydrogenase complex mutants of *Pseudomonas aeruginosa* PAO. *J. Gen. Microbiol.* **120**, 385–392 (1980).
31. La Rosa, R., Behrends, V., Williams, H. D., Bundy, J. G. & Rojo, F. Influence of the Crc regulator on the hierarchical use of carbon sources from a complete medium in Pseudomonas. *Environ. Microbiol.* **18**, 807–818 (2016).
32. Molina, L., Rosa, R., La, Nogales, J. & Rojo, F. *Pseudomonas putida* KT2440 metabolism undergoes sequential modifications during exponential growth in a complete medium as compounds are gradually consumed. *Environ. Microbiol.* **21**, 2375–2390 (2019).
33. Škerlová, J., Berndtsson, J., Nolte, H., Ott, M. & Stenmark, P. Structure of the native pyruvate dehydrogenase complex reveals the mechanism of substrate insertion. *Nat. Commun.* **12**, 5277 (2021).
34. Marvig, R. L., Sommer, L. M., Molin, S. & Johansen, H. K. Convergent evolution and adaptation of *Pseudomonas aeruginosa* within patients with cystic fibrosis. *Nat. Genet.* **47**, 57–64 (2015).
35. La Rosa, R., Johansen, H. K. & Molin, S. Convergent metabolic specialization through distinct evolutionary paths in *Pseudomonas aeruginosa*. *mBio* **9**, e00269–18 (2018).
36. Othman, D. S. M. P., Schirra, H., McEwan, A. G. & Kappler, U. Metabolic versatility in *Haemophilus influenzae*: a metabolomic and genomic analysis. *Front. Microbiol.* **5**, 69 (2014).
37. Behrends, V. et al. Metabolite profiling to characterize disease-related bacteria: gluconate excretion by *Pseudomonas aeruginosa*

mutants and clinical isolates from cystic fibrosis patients. *J. Biol. Chem.* **288**, 15098–15109 (2013).
38. Jurado-Martín, I., Sainz-Mejías, M. & McClean, S. *Pseudomonas aeruginosa*: an audacious pathogen with an adaptable arsenal of virulence factors. *Int. J. Mol. Sci.* **22**, 1–37 (2021).
39. O'donnell-Tormey, J., Nathan, C. F., Lanks, K., Deboer, C. J. & De La Harpe, J. Secretion of pyruvate. An antioxidant defense of mammalian cells. *J. Exp. Med.* **165**, 500–514 (1987).
40. Galli, F. et al. Oxidative stress and antioxidant therapy in cystic fibrosis. *Biochim. Biophys. Acta Mol. Basis Dis.* **1822**, 690–713 (2012).
41. Fu, T., Wright, R. C. T., Gifford, D. R., Knight, C. G. & Brockhurst, M. A. Inflammation-like environments limit the loss of quorum sensing in *Pseudomonas aeruginosa*. *mSystems* **10**, e0172224 (2025).
42. da Cruz Nizer, W. S. et al. Oxidative stress response in *Pseudomonas aeruginosa*. *Pathogens* **10**, 1187 (2021).
43. Dacheux, D. et al. Activation of the *Pseudomonas aeruginosa* type III secretion system requires an intact pyruvate dehydrogenase aceAB operon. *Infect. Immun.* **70**, 3973–3977 (2002).
44. Cuzick, A., Stirling, F. R., Lindsay, S. L. & Evans, T. J. The type III pseudomonal exotoxin U activates the c-Jun NH 2-terminal kinase pathway and increases human epithelial interleukin-8 production. *Infect. Immun.* **74**, 4104–4113 (2006).
45. Soto-Heredero, G., Gómez de las Heras, M. M., Gabandé-Rodríguez, E., Oller, J. & Mittelbrunn, M. Glycolysis—a key player in the inflammatory response. *FEBS J.* **287**, 3350–3369 (2020).
46. Abusalamah, H., Reel, J. M. & Lupfer, C. R. Pyruvate affects inflammatory responses of macrophages during influenza A virus infection. *Virus Res.* **286**, 198088 (2020).
47. Koprivica, I., Djedovic, N., Stojanović, I. & Miljković, Đ. Ethyl pyruvate, a versatile protector in inflammation and autoimmunity. *Inflamm. Res.* **71**, 169–182 (2022).
48. Rossi, E., Falcone, M., Molin, S. & Johansen, H. K. High-resolution in situ transcriptomics of *Pseudomonas aeruginosa* unveils genotype independent patho-phenotypes in cystic fibrosis lungs. *Nat. Commun.* **9**, 3459 (2018).
49. Grayczyk, J. P., Harvey, C. J., Laczkovich, I. & Alonzo, F. A lipoylated metabolic protein released by *Staphylococcus aureus* suppresses macrophage activation. *Cell Host Microbe* **22**, 678–687.e9 (2017).
50. Wang, X. et al. Conserved moonlighting protein pyruvate dehydrogenase induces robust protection against *Staphylococcus aureus* infection. *Proc. Natl. Acad. Sci. USA* **121**, e2321939121 (2024).
51. Turner, K. H., Wessel, A. K., Palmer, G. C., Murray, J. L. & Whiteley, M. Essential genome of *Pseudomonas aeruginosa* in cystic fibrosis sputum. *Proc. Natl. Acad. Sci. USA* **112**, 4110–4115 (2015).
52. Fortuna, A. et al. The *Pseudomonas aeruginosa* DksA1 protein is involved in H_2O_2 tolerance and within-macrophages survival and can be replaced by DksA2. *Sci. Rep.* **12**, 10404 (2022).
53. Walters, M. S. et al. Generation of a human airway epithelium derived basal cell line with multipotent differentiation capacity. *Respir. Res.* **14**, 135 (2013).
54. Laborda, P. et al. Mutations in the efflux pump regulator MexZ shift tissue colonization by *Pseudomonas aeruginosa* to a state of antibiotic tolerance. *Nat. Commun.* **15**, 2584 (2024).
55. Goltermann, L. et al. Macrolide resistance through uL4 and uL22 ribosomal mutations in *Pseudomonas aeruginosa*. *Nat. Commun.* **15**, 8906 (2024).
56. Katoh, K., Rozewicki, J. & Yamada, K. D. MAFFT online service: multiple sequence alignment, interactive sequence choice and visualization. *Brief. Bioinform.* **20**, 1160–1166 (2018).
57. Wirth, N. T., Funk, J., Donati, S. & Nikel, P. I. QurvE: user-friendly software for the analysis of biological growth and fluorescence data. *Nat. Protoc.* **18**, 2401–2403 (2023).

Acknowledgements

We thank the Infection Microbiology group for their insightful comments and discussion, especially Alexander Frederick Melanson for his support with macrophage assays. The Basal Cell Immortalized Non-Smoker 1.1 (BCi-NS1.1) cell line was a gift from Professor Ronald G. Cristal (Weil Cornell Medical College, New York, USA).

Author contributions

R.L.R. and P.L. designed the project. S.L., L.M., and P.L. performed the experiments. R.L.R. performed the data analysis. H.K.J. provided strains and clinical data. H.K.J. and S.M. provided funding. P.L. and R.L.R. verified the data and wrote the first draft of the paper. All authors approved the final version of the manuscript.

Funding

This research was funded by the "Novo Nordisk Foundation Center for Biosustainability (CfB)" grant number NNF10CC1016517, by the Challenge Grant NNF19OC0056411 from the Novo Nordisk Foundation, and a grant from the John and Birthe Meyer Foundation to H.K.J. P.L. is the recipient of an ERS/EU RESPIRE4 Marie Skłodowska-Curie Postdoctoral Research Fellowship (Ref. nr: R4202305-01047; this project has received funding from the European Respiratory Society and the European Union's H2020 research and innovation programme under the Marie Skłodowska-Curie grant agreement No. 847462).

Competing interests

The authors declare no competing interests.

Additional information

Supplementary information The online version contains Supplementary material available at https://doi.org/10.1038/s41467-026-75330-z.

Correspondence and requests for materials should be addressed to Pablo Laborda or Ruggero La Rosa.

Peer review information *Nature Communications* thanks the anonymous reviewers for their contribution to the peer review of this work. A peer review file is available.

Reprints and permissions information is available at http://www.nature.com/reprints

Publisher's note Springer Nature remains neutral with regard to jurisdictional claims in published maps and institutional affiliations.

Open Access This article is licensed under a Creative Commons Attribution-NonCommercial-NoDerivatives 4.0 International License, which permits any non-commercial use, sharing, distribution and reproduction in any medium or format, as long as you give appropriate credit to the original author(s) and the source, provide a link to the Creative Commons licence, and indicate if you modified the licensed material. You do not have permission under this licence to share adapted material derived from this article or parts of it. The images or other third party material in this article are included in the article's Creative Commons licence, unless indicated otherwise in a credit line to the material. If material is not included in the article's Creative Commons licence and your intended use is not permitted by statutory regulation or exceeds the permitted use, you will need to obtain permission directly from the copyright holder. To view a copy of this licence, visit http://creativecommons.org/licenses/by-nc-nd/4.0/.

© The Author(s) 2026